Research Article

Hajer A. Ali* and Nahida J. Hameed

# The study of the particle size effect on the physical properties of $TiO_2$/cellulose acetate composite films

https://doi.org/10.1515/jmbm-2022-0019
received October 28, 2021; accepted April 09, 2022

**Abstract:** The cast method was used to synthesize cellulose acetate (CA)/titanium oxide ($TiO_2$) composites by varying $TiO_2$ particle sizes at different weight ratios of 1, 1.5, 2, 2.5, and 3 wt%. The relationship between structural diversity and performance was explored. Microstructures and chemical composition of as-prepared composite films were revealed using field-emission scanning electron microscopy and Fourier-transform infrared spectroscopy. The tensile strength increased from 46.8 MPa for pure CA to 54.7 MPa for the CA-1% micro-$TiO_2$ composite and 81.7 MPa for the CA-2% nano-$TiO_2$ composite, according to the mechanical properties. The tensile strength decreased due to some degrees of agglomeration of filler particles above a critical content. UV-vis transmittance spectra showed that pure CA was almost transparent, CA-micro-$TiO_2$ films were less transparent than pure CA, and CA-nano-$TiO_2$ films could efficiently block the light. XRD diffraction for the synthesized membranes was performed. The patterns of micro-$TiO_2$ and nano-$TiO_2$ were shown as $2\theta = 25°$ for the anatase phase and $2\theta = 18.5$ for the pure CA film, respectively. The hydrophilicity of films was also measured using the sessile drop technique. The contact angle value for the pure CA was 61.3°. As the amount of $TiO_2$ added to the films increased, the contact angles of the CA-micro $TiO_2$ and CA-nano $TiO_2$ films reduced from 53.2° to 29° and from 51.5° to 27°, respectively. The produced films' improved wettability indicated that these films could be employed as filters.

**Keywords:** biodegradable, cellulose acetate, mechanical properties, nanocomposite, titanium oxide

## 1 Introduction

Traditional synthetic polymers, such as polyethylene (PE), polyvinyl chloride (PVC), polypropylene (PP), polyterephthalate (PET), and polyurethane (PU) which have been available for decades, have been applied as food packaging, medicine, waterproofing, and coating materials. Their superior properties such as good mechanical performance, low density, low cost, high chemical stability and a wide range of fabrication techniques make them a typical choice for many industrial applications [1]. However, the only drawback is the low degradation rate of their wastes, which is growing rapidly and may eventually become a serious environmental challenge. Several methods and techniques have emerged to overcome this challenge such as recycling and reusing polymer waste [2–4]. However, the most efficient way is to develop environmentally friendly biodegradable polymers such as chitosan, starch, and cellulose as an alternative to the traditional materials.

Cellulose acetate (CA) is a common natural organic polymer that can be transformed into high-end derivatives [5], but some of its properties, such as good appearance, biodegradability, and great durability, make it more favorable than its derivatives [6]. Using the esterification technique, CA can be produced from naturally produced cellulose substances including wood, cotton, and rice husk, as well as recyclable materials like paper [7,8]. Because of its biodegradation, nontoxicity, transparency, hydrophilicity and cost effectiveness, it appears to be a viable material for a variety of uses such as filters, drug delivery agents, food packaging films, and medical implants [9]. However, due to its brittleness and high sensitivity to moisture, it is not suitable for a wider range of applications in composite films [10]. Composite films

* **Corresponding author: Hajer A. Ali,** Materials Science Branch, Department of Applied Sciences, University of Technology – Iraq, Baghdad, Iraq; Mesopotamian State Company of Seeds, Ministry of Agriculture, Baghdad, Iraq, e-mail: as.18.47@grad.uotechnology.edu.iq
**Nahida J. Hameed:** Materials Science Branch, Department of Applied Sciences, University of Technology – Iraq, Baghdad, Iraq, e-mail: nahidajoumaa61@yahoo.com

that were developed overcome this difficulty by mixing inorganic oxide ($TiO_2$) with a CA solution. Because of its steady nature, availability, and suitability for various applications, $TiO_2$ has been the focus of many studies [11,12]. Several research teams have used the phase reversal method to create various polymer–$TiO_2$ composite films. Water flow and antifouling properties were greatly improved by polyethersulfone/$TiO_2$ composite ultrafiltration films [13]. The electrospinning process can create PU/$TiO_2$/fly ash composite water purification films and CA–$TiO_2$ films for water treatment applications [14,15]. To meet the needs of various industries, researchers created polyacrylonitrile–$TiO_2$ [16], $TiO_2$/polyvinyl alcohol [17], and $TiO_2$/PVDF composite films [18]; polysulfone enhanced films with $TiO_2$ nanofibers [19]; CA/MIL-53-$NH_2$ film for efficient chlorpyrifos' elimination [20]; CA/Ti-MIL-$NH_2$ films for a chosen pharmaceutical residue removal [21]; CA/Cu-MOF films for selective dimethoate pesticide removal from wastewaters [22]; and CA/employable metal (Ag and Pd)/MIL-125-$NH_2$ films for reducing nitro-aromatics reducing via visible-light photocatalysis [23]. The current study focuses on the synthesis and application of CA films that combine micro- or nano-$TiO_2$ nanoparticles. It is different from previous studies because it incorporates different particle sizes and processes and conducts various examinations for filter application. The physical, chemical, and structural properties of CA/micro- or nano-$TiO_2$ composite films, as well as XRD patterns and contact angles, are investigated.

# 2 Materials and methods

## 2.1 Materials

In this work, CA (CDH India; acetyl content, 29–45%; maximum limit of impurities, 0.1%; free acid [as acetic acid], 5.0%; sulfated ash loss on drying at 105°C, 0.1%) and AR/ACS-grade acetone (2-propanone, dimethylketone; CDH India) (MW: 58.08) were utilized.

Titanium oxide nanoparticles/nanopowders ($TiO_2$, anatase, 99.5%) of particle size (20–80) nm were purchased from Skyspring (USA). Micro-$TiO_2$ with particle sizes ranging from 100 to 2,000 nm was supplied by Nanoshel (USA).

## 2.2 Composite polymer solution preparation

The primary solution of CA was made by dissolving 7 g of CA powder in 100 mL of acetone. After 8 h of stirring with a magnetic stirrer, the solution was cast in a glass Petri dish, and the final film was obtained after 48 h.

At different weight ratios of 1, 1.5, 2, 2.5, and 3 wt%, the micro-$TiO_2$ or nano-$TiO_2$ solution was added to CA powder. The solution was cast on a glass Petri dish and permitted to dry for 48 h after being agitated until it became homogenous. Figure 1 depicts the preparation process.

# 3 Characterization

The morphologies of the composite surface and powder were examined with field-emission scanning electron microscopy ([FESEM] Zeiss Sigma 300-HV, Germany). The mechanical characteristics of CA and composite thick films were measured by tensile tests using a universal testing machine (UTM) UE3450 from Laryee Technology Co., Ltd., China. The films were cut to 12 mm × 60 mm, and thickness was measured by a digital micrometer with ±1 µm accuracy. All of the tests were carried out at room temperature (about 27°C), with a cross-head speed of 5 mm/min being utilized to measure the cellulose-based films and a stress–strain curve being produced. A well-known standard procedure was used to determine Young's modulus, elongation at break, and ultimate tensile strength.

Fourier-transform infrared (FTIR) spectra were obtained by a Japan-made SHIMADZU-8400S FTIR spectrometer. The spectra were obtained in the wavenumber range of 400–4,000 $cm^{-1}$, at 4 $cm^{-1}$ resolution. The samples were prepared as tablets by mixing with KBr powder.

UV-vis spectra were obtained by Japan-made Shimadzu spectrometer. The wavenumber range of 200–1,100 Nm was utilized to obtain the spectra.

An X-ray diffractometer (BRUKER, D8 advance, USA) with Cu kα radiation operates at 40 kV/30 mA.

The optical system used to measure contact angles was from Holmarc Opto-Mechatronics Pvt. Ltd., India, with an automated dispenser and software for static and dynamic contact angle measurements. When a drop of water is dropped on the film's surface, it spreads due to interactions between the solid surface and the water. The water contact angle will be measured to determine the surface's wettability.

# 4 Results and discussion

## 4.1 SEM analysis

SEM micrographs and particle size distributions of micro- and nano-$TiO_2$ powders are shown in Figures 2 and 3, respectively. As clearly shown, the micro-$TiO_2$ powder

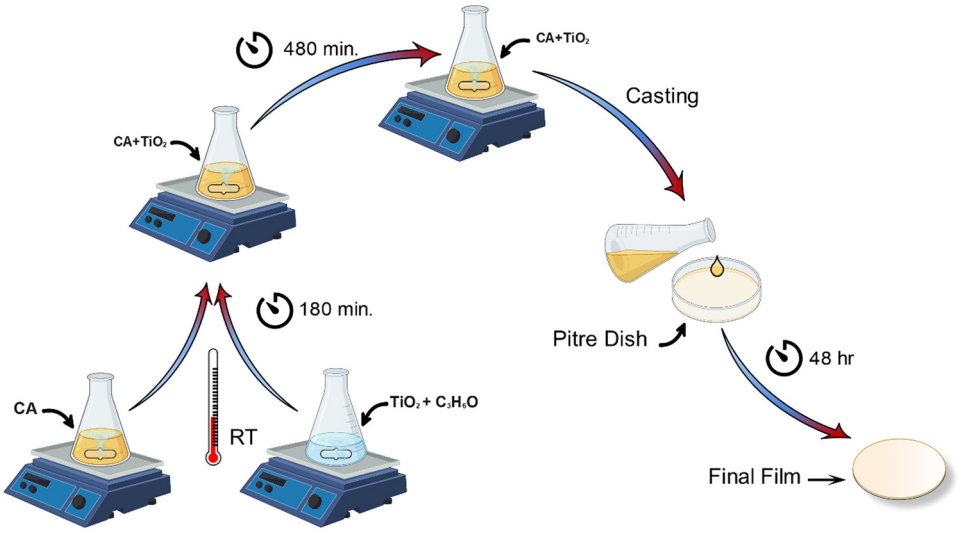


**Figure 1:** Schematic diagram of the preparation process for films.

covered a wide range of particle size from about 0.1 to 2 µm. The particles also have a regular crystalline morphology with smooth surfaces and sharp edges. On the other hand, nano-$TiO_2$ powder has a very fine particle size with a narrow distribution of about 20–80 Nm. Fine particles have a high degree of agglomeration due to their high surface area, so a more sophisticated dispersion technique will be required to prevent agglomeration and achieve a higher homogeneity of the particle distribution within the CA matrix.

## 4.2 Tensile test

The mechanical properties of polymer systems depend on the intermolecular force, stiffness, and molecular symmetry of polymer systems [24]. Figure 4 shows the stress–strain curves for $TiO_2$/CA composite films with different weight ratios (1, 1.5, 2, 2.5, and 3 wt%) of micro-$TiO_2$ and nano-$TiO_2$. The good distribution of inorganic fillers in the (CA) polymer matrix was responsible for improving mechanical properties by up to 1 wt% for micro-$TiO_2$/CA and up to 2 wt% for nano-$TiO_2$/CA [25–27]. Polymers with a high degree of crystallinity, crosslinking, or rigid chains had a high strength or limited extendibility, resulting in a high yield modulus, a high stress at peak value, and a low elongation value. Due to the electrostatic interactions between the ester atoms of one chain and the hydroxyl atoms of another, CA becomes a rigid, strong material that exhibits dipole–dipole attraction. The dipole–dipole attraction, which reaches its maximum magnitude, was associated with improved mechanical characteristics. The increase in strength can be attributed to a greater capacity of the filler to attach to the matrix, which resulted in less sliding between the composite layers when stress was applied [28,29].

The tensile strength reduced due to some degrees of agglomeration of filler particles above the critical content

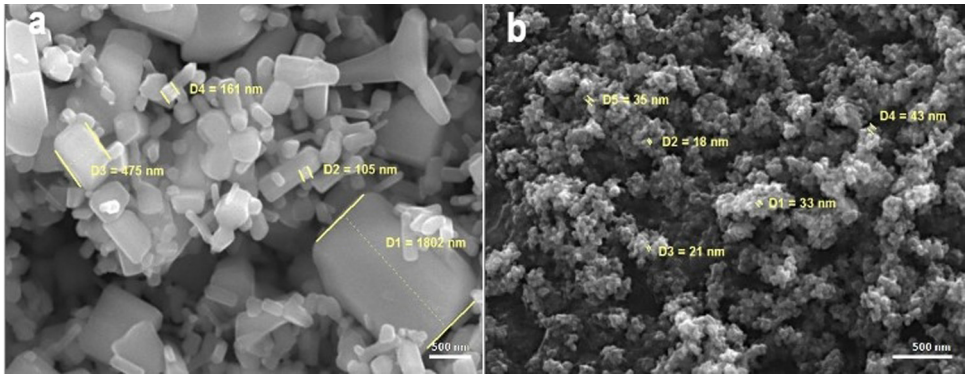


**Figure 2:** SEM images of (a) micro-$TiO_2$ and (b) nano-$TiO_2$.

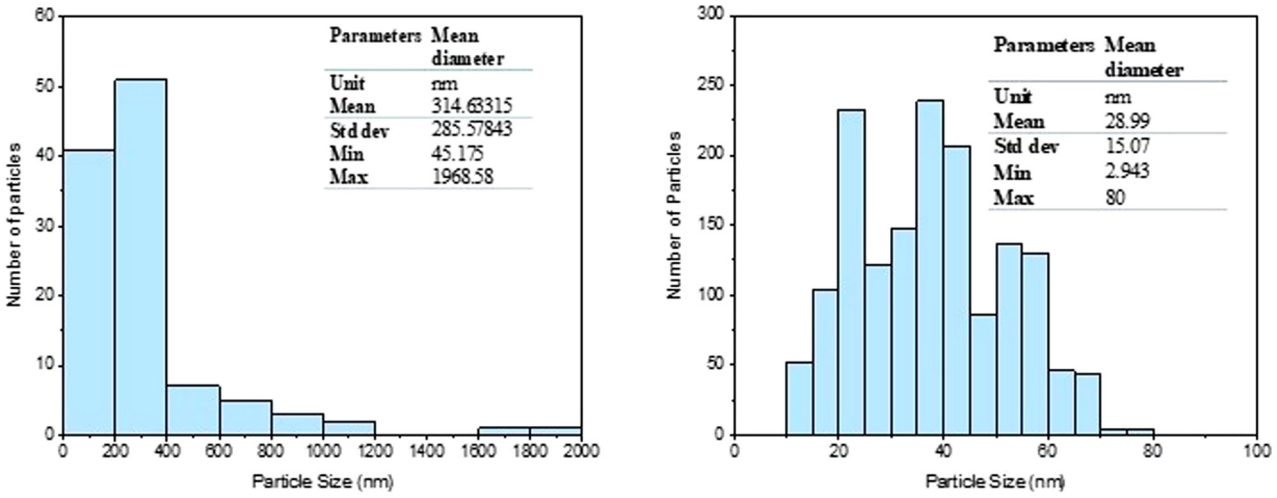


**Figure 3:** Particle size distribution of (a) micro-$TiO_2$ and (b) nano-$TiO_2$.

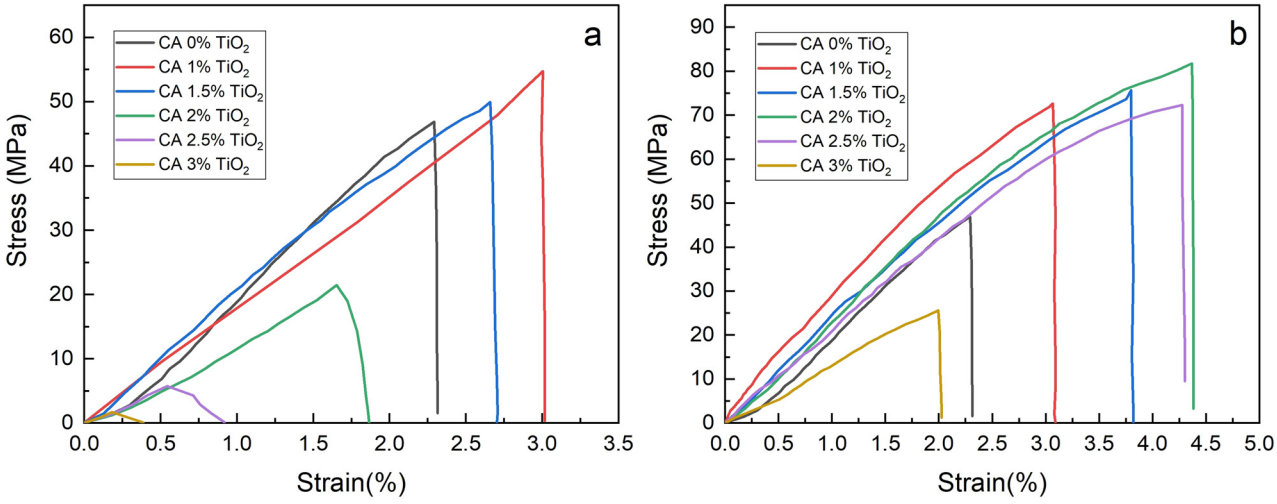


**Figure 4:** Stress–strain curve of (a) micro- and (b) nano-$TiO_2$-filled CA films.

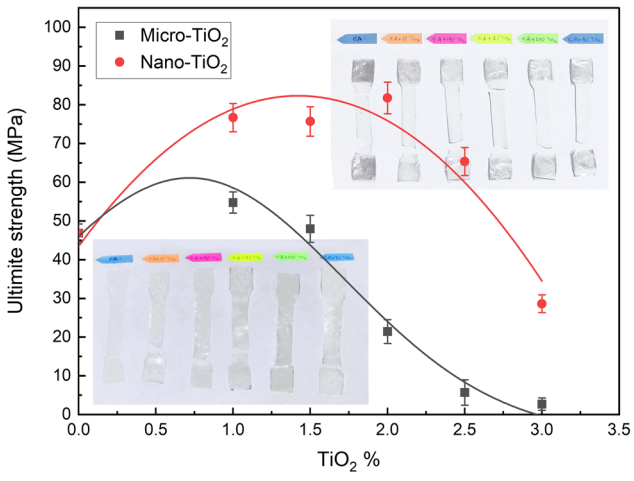


**Figure 5:** Ultimate tensile strength of CA films with different $TiO_2$ contents.

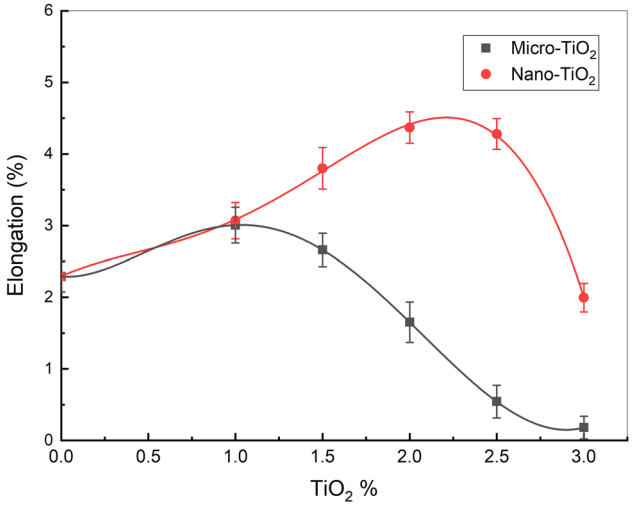


**Figure 6:** Elongation of micro- and nano-$TiO_2$-filled CA films.

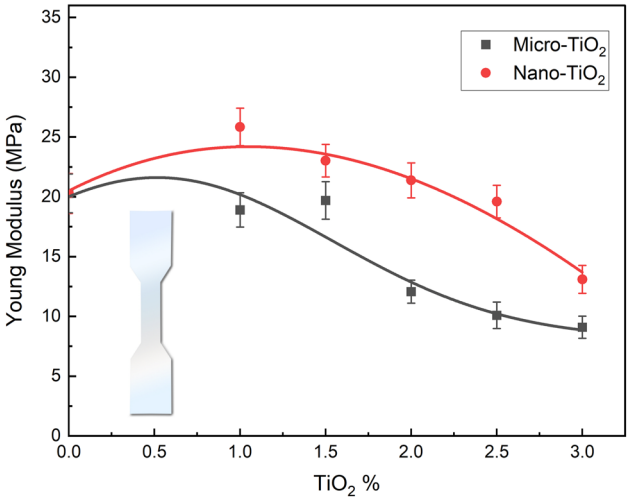


**Figure 7:** Young's modulus of micro- and nano-$TiO_2$-filled CA films.

and an increase in inhomogeneity [25,26]. The lack of interfacial adhesion between the polymer and the fillers was responsible for the decrease in tensile strength [29].

As seen from Figures 5–7, the tensile strength after incorporation of (nano-$TiO_2$) was higher than that after incorporation of (micro-$TiO_2$), which was attributed to a difference in the reinforcing or strengthening mechanism. The term "micro" refers to the fact that the particle–matrix interaction is too small to be treated at the atomic or molecular level. Most of these composites have a harder and stiffer particulate phase than the matrix. The reinforcing particles tend to retain the mobility of the matrix phase in the vicinity of these reinforcing particles. In essence, the matrix transfers a portion of applied stress to the particles that are only carrying a part of the load. The particle sizes are within a range of 10–100 nm. At an atomic or molecular level, the matrix interaction is strengthened. The matrix bears the majority of the applied load, but the small dispersion particles hinder or impede dislocation movement. Plastic deformation is reduced, resulting in an enhanced yield and tensile strength [30]. Both tensile strength and elongation were improved at the fixed levels of 1 wt% (micro-$TiO_2$) and 2 wt% (nano-$TiO_2$) loadings, as shown in Figures 4 and 5. However, above that level of loading, the tensile strength and elongation decreased.

The general behavior of Young's modulus was found to depend on the elongation and ultimate strength according to the filler contents and the homogeneity of particle distribution within the CA matrix. This result agrees with those of Rajeswari *et al.* [31].

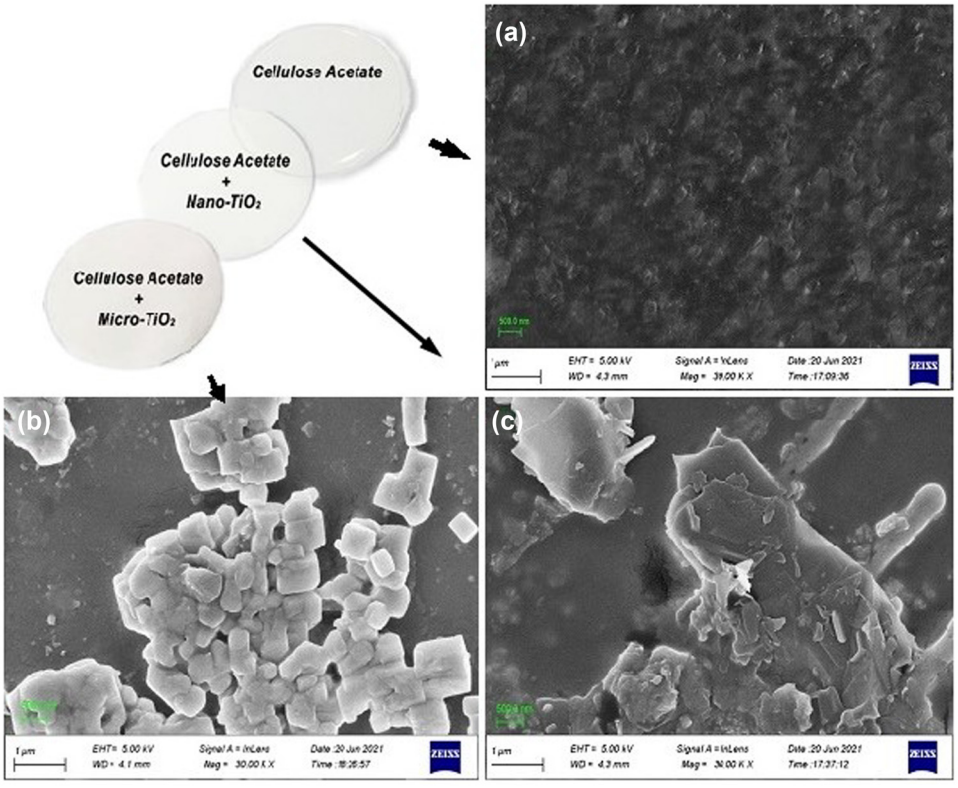


**Figure 8:** FESEM images: (a) CA, (b) CA + 1 wt% micro-$TiO_2$, and (c) CA + 2 wt% nano-$TiO_2$.

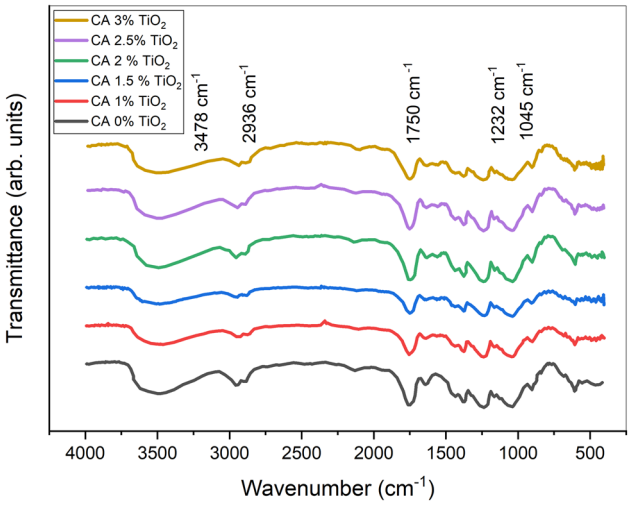


**Figure 9:** FTIR spectra of micro-$TiO_2$-based CA.

## 4.3 Membrane morphology

Figure 8 shows the FESEM images of CA, CA-1 wt% micro-$TiO_2$, and CA-2 wt% nano-$TiO_2$ films. The film of CA is obtained as a rough pattern with a homogeneity surface [32]. At 1 wt% micro-$TiO_2$, the existence of a small bright region has been observed in the film with an indication of particle agglomeration on the surface. Hence, the mechanical properties of the composites decrease because of these agglomerated particles [33]. There were no aggregation regions in the CA matrix where nanoparticles were dispersed. This could be due to the efficiency of nanoparticle dispersion in the CA matrix, which would explain the improvement in the films' tensile properties [34,35]. This result agrees with that of Gao *et al.* [36].

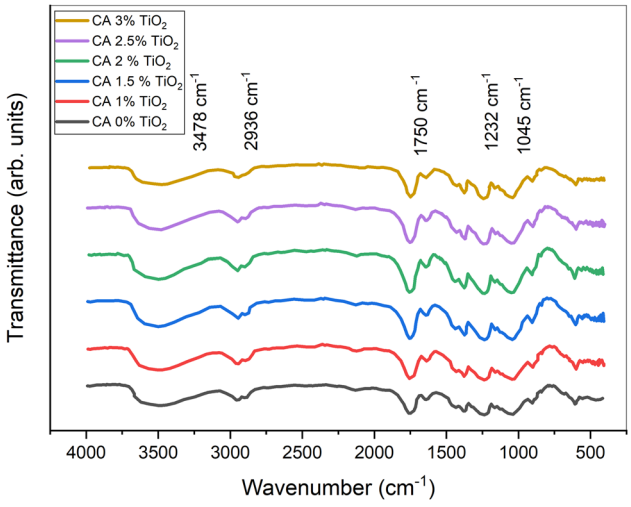


**Figure 10:** FTIR spectra of nano-$TiO_2$-based CA.

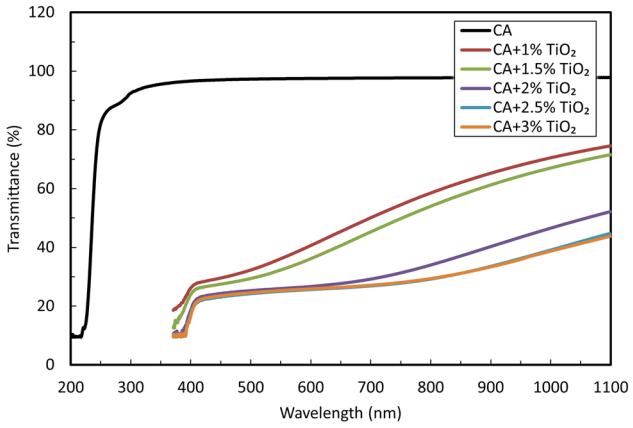


**Figure 11:** UV-vis spectroscopy of micro-$TiO_2$-based CA.

## 4.4 FTIR spectroscopy

Figures 9 and 10 show the FTIR spectra of pure CA films and CA films containing 1, 1.5, 2, 2.5, and 3 wt% micro-$TiO_2$ and nano-$TiO_2$, respectively. The film spectrum is characterized by the presence of bands at 1,741 $cm^{-1}$ (steric carbonyl stretching), 3,478 $cm^{-1}$ (cellulose OH stretching), and 2,936 $cm^{-1}$ (CH stretching) [37]. The bands at 2,936 $cm^{-1}$ (CH stretching), 3,478 $cm^{-1}$ (OH stretching), 1,741 $cm^{-1}$ (steric carbonyl stretching), 1,232 $cm^{-1}$, and 1,045 $cm^{-1}$ (C–O stretching), all increased when micro-$TiO_2$ or nano-$TiO_2$ was added. Inserting $TiO_2$ into CA may have strengthened the interactions between two compounds at the region of the band that exhibited these properties since the chemical structure of $TiO_2$ is an oxide with O–Ti–O bonding. $TiO_2$ bonding is represented by peaks at 400–600 $cm^{-1}$ and 750 $cm^{-1}$ [38,39]. Carbanion and hydroxyl groups have peaks centered at 1,750 and 3,478 $cm^{-1}$, respectively [38]. This result agrees with that of Prakash *et al.* [40].

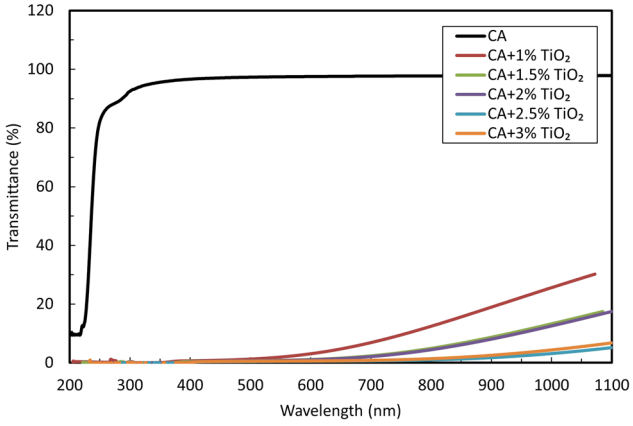


**Figure 12:** UV-vis spectroscopy of nano-$TiO_2$-based CA.

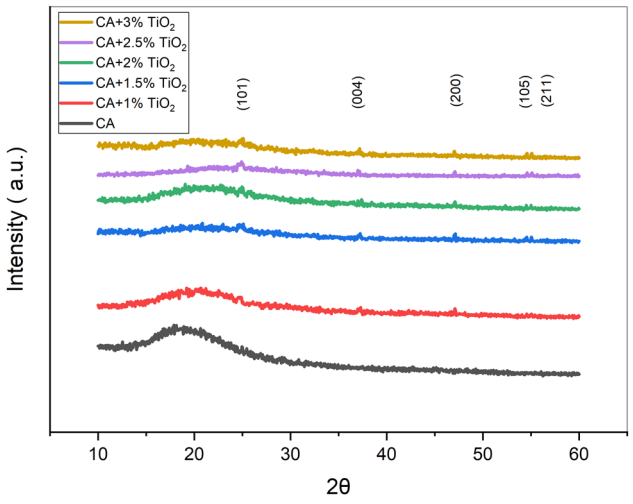


**Figure 13:** XRD pattern of micro-$TiO_2$-based CA.

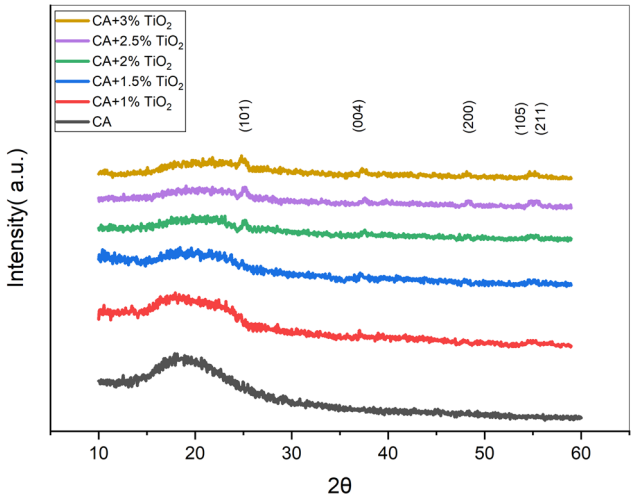


**Figure 14:** XRD pattern of nano-$TiO_2$-based CA.

## 4.5 UV-vis spectroscopy

UV-vis spectroscopy gives useful information on the reflectance, absorbance, and transmittance of polymeric materials [41]. It is well known that CAs are very important polymers because they have excellent optical properties, such as great translucency [42]. Figures 11 and 12 depict the UV-vis Transmittance spectra of pure CA film and CA films containing 1, 1.5, 2, 2.5, and 3 wt% micro-$TiO_2$ and nano-$TiO_2$, respectively. The transmittance spectra of pure CA were almost transparent in all regions. CA-micro-$TiO_2$ films were less transparent than pure CA, while CA-nano-$TiO_2$ films could efficiently block the lights. This could be attributed to the difference between micro- and nano-$TiO_2$ particles, since particle–matrix interactions that lead to strengthening occur at an atomic or molecular level for small particles but not for large particles [30]. Hence, UV-vis spectra revealed that the transmittance was mostly in the visible region, with a small UV wavelength range. This result agrees with that of Sharma *et al.*, who studied

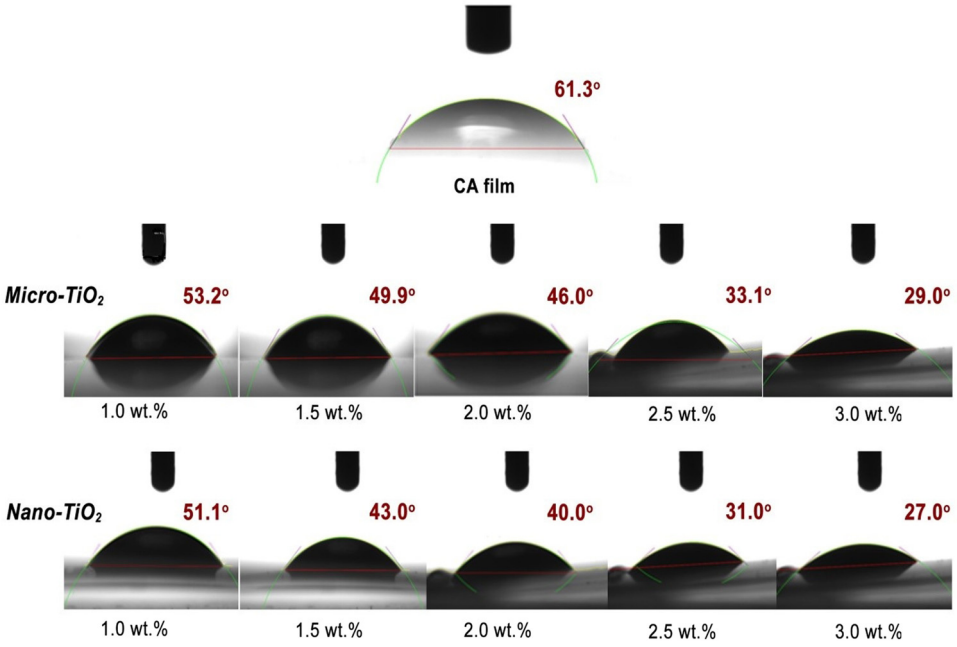


**Figure 15:** Water contact angles for CA nanocomposite thick films with various $TiO_2$ contents.

the optical properties of CA and CA-based lignocelluosic nanofiber. On CA films and with lower lignin concentration, there was an enhancement in transmittance [43].

### 4.6 X-ray diffraction (XRD)

Figures 13 and 14 show the X-ray diffraction patterns of pure CA film and CA films containing 1, 1.5, 2, 2.5, and 3 wt% micro-$TiO_2$ and nano-$TiO_2$, respectively. The patterns of micro-$TiO_2$ and nano-$TiO_2$ were shown as $2\theta = 25°$ anatase, matching with JCPDS card no. 21-1272, where these are characteristic crystalline peaks [44]. According to these results, it was indicated that $TiO_2$ is largely composed of anatase. Among the other types, anatase has excellent stability, antifouling properties, and hydrophilic nature, all of which are important filtration film characteristics. Furthermore, this can be used to alter films [45]. As seen in Figures 13 and 14, the wide peak observed below $2\theta = 18.5°$ for the pure CA film corresponds to the semi-crystalline arrangement of the CA film [46]. The strong and sharp characteristic peaks in the composite film indicate the good crystallinity of the manufactured films. This result agrees with that of Das and Gebru [15].

### 4.7 Water contact angle

The hydrophilicity of the films is determined by measuring the water contact angle [47]. Water contact angles for CA are represented in Figure 15. CA-micro-$TiO_2$ and CA-nano-$TiO_2$ at different percentages of 1, 1.5, 2, 2.5, 3 wt% are represented in the figure. The CA film had the lowest surface wettability of all the produced films, with a contact angle of 61.3°, due to its hydrophilic nature, whereby low surface wettability leads to a high contact angle, and *vice versa* [48]. The contact angle of the CA-micro-$TiO_2$ and CA-nano-$TiO_2$ composite films reduced dramatically, from 53.2° to 29° and from 51.5° to 27°, respectively, due to the presence of the anatase phase of $TiO_2$, which was less hydrophilic than CA. The hydrophilicity of the prepared films has noticeably improved as the micro- and nanoparticle content increased. This result agrees with that of Neelapala *et al.*, who found similar results [49].

## 5 Conclusion

CA–$TiO_2$ (micro and nano) composite films were prepared using the casting method in this investigation. The effects of micro- and nano-$TiO_2$ on the microstructure morphology of casted CA thick films were examined. FESEM images of CA, CA + 1 wt% micro-$TiO_2$, and CA + 2 wt% nano-$TiO_2$ revealed that both types of particles exhibit a high degree of particle dispersion homogeneity within the CA matrix. The addition of micro- or nano-$TiO_2$ increased the ultimate tensile strength and Young's modulus up to 1 wt% for micro and 2 wt% for nanocomposite films but then slightly decreased along with increasing $TiO_2$ content, according to the tensile test results. FTIR spectra demonstrated the interaction between CA and micro- or nano-$TiO_2$. UV-vis transmittance spectra showed that pure CA was almost transparent, CA-micro-$TiO_2$ films were less transparent than pure CA, while CA-nano-$TiO_2$ films were dim. XRD diffraction for the composite films was performed. The patterns of micro-$TiO_2$ and nano-$TiO_2$ were presented as $2\theta = 25°$ for anatase phase and $2\theta = 18.5°$ for pure CA film, respectively. The addition of micro- or nano-$TiO_2$ from 1 to 3% of the total weight resulted in an increase in hydrophilicity. The prepared films could be used in filter applications due to their hydrophilicity.

**Acknowledgment:** The authors express their appreciation to Senior Researcher Ali J. Addie, Eng. Mukhallad H. Shwaish, Dr. Mohammed S. Ali, Dr. Mohammed S. Mohammed, Asst.Tech. Amani K. Hussein, Dr. Hanaa J. Kadhim for their help in examinations and our appreciation to all staff of the Journal.

**Funding information:** The authors state no funding involved.

**Author contributions:** All authors have accepted responsibility for the entire content of this manuscript and approved its submission.

**Conflict of interest:** There are no conflicts of interest declared by researchers.

## References

[1] Cai H-T, Xu H, Tang C, Li J, Yang Z-Y, Ye S-H, et al. Intrinsic ambipolar transport for the traditional conducting or hole transport ionic blend polymer PEDOT:PSS. Polymer (Guildf). 2019;180:121732.

[2] García-Arroyo P, Arrieta MP, Garcia-Garcia D, Cuervo-Rodríguez R, Fombuena V, Mancheño MJ, et al. Plasticized poly (lactic acid) reinforced with antioxidant covalent organic frameworks (COFs) as novel nanofillers designed for non-migrating active packaging applications. Polymer (Guildf). 2020;196:122466.

[3] Wen L, Liang Y, Lin Z, Xie D, Zheng Z, Xu C, et al. Design of multifunctional food packaging films based on carboxymethyl chitosan/polyvinyl alcohol crosslinked network by using citric acid as crosslinker. Polymer (Guildf). 2021;230:124048.
[4] Nzenguet AM, Aqlil M, Essamlali Y, Amadine O, Snik A, Larzek M, et al. Novel bionanocomposite films based on graphene oxide filled starch/polyacrylamide polymer blend: structural, mechanical and water barrier properties. J Polym Res. 2018;25(4):86.
[5] Kamel R, El-Wakil NA, Dufresne A, Elkasabgy NA. Nanocellulose: From an agricultural waste to a valuable pharmaceutical ingredient. Int J Biol Macromol. 2020;163:1579–90.
[6] Cindradewi AW, Bandi R, Park C-W, Park J-S, Lee E-A, Kim J-K, et al. Preparation and characterization of cellulose acetate film reinforced with cellulose nanofibril. Polymers (Basel). 2021 Sep;13:17.
[7] Sharma A, Giri SK, Kartha KPR, Sangwan RS. Value-additive utilization of agro-biomass: preparation of cellulose triacetate directly from rice straw as well as other cellulosic materials. RSC Adv. 2017;7(21):12745–52.
[8] Candido RG, Godoy GG, Gonçalves A. Characterization and application of cellulose acetate synthesized from sugarcane bagasse. Carbohydr Polym. 2017;167:280–9.
[9] Oribe A, Shabbeb K, Hassan A. Synthesis and characteristics of acetylated corn cob powder/unsaturated polyester composite. Eng Technol J. 2020;38(7):1084–95.
[10] Bahjat H, Ismail R, Sulaiman G, Jabir M. Magnetic field-assisted laser ablation of titanium dioxide nanoparticles in water for anti-bacterial applications. J Inorg Organomet Polym Mater. 2021;31(1):3649–56.
[11] Wang H, Ding K. Effect of self-made $TiO_2$ nanoparticle size on the performance of the PVDF composite membrane in MBR for landfill leachate treatment. J Membr. 2022;12(2):216.
[12] Saleh R, Salman O, Dawood M. Physical investigations of titanium dioxide nanorods film prepared by hydrothermal technique. J Appl Sci Nanotechnol. 2021;1(3):32–41.
[13] Singh S, Karwa V, Marathe KV. UV-assisted surface modification of polyethersulfone (PES) membrane using $TiO_2$ nanoparticles. J Membr Water Treat. 2018;9(6):393–403.
[14] Joo Kim H, Raj Pant H, Hee Kim J, Jung Choi N, Sang, Kim C. Fabrication of multifunctional $TiO_2$-fly ash/polyurethane nanocomposite membrane via electrospinning. Ceram Int. 2014;40(2):3023–9.
[15] Das C, Gebru KA. Cellulose acetate modified titanium dioxide ($TiO_2$) nanoparticles electrospun composite membranes: fabrication and characterization. J Inst Eng Ser E. 2017;98(2):91–101.
[16] Wang Q, Wang T, Lv Z, Cui M, Zhao Z, Cao X, et al. $TiO_2$ sol–gel coated PAN/O-MMT multi-functional composite nanofibrous membrane used as the support for laccase immobilization: synergistic effect between the membrane support and enzyme for dye degradation. Polymers (Basel). 2020 Jan;12:1.
[17] Dhokne(Pathare) R, More(Jadhav) S, Pathare N. Structural and dielectric properties of polyvinyl alcohol-$TiO_2$ doped thin films. Macromol Symp. 2021;400(1):2100014.
[18] Erusappan E, Thiripuranthagan S, Radhakrishnan R, Durai M, Kumaravel S, Vembuli T, et al. Fabrication of mesoporous $TiO_2$/PVDF photocatalytic membranes for efficient photocatalytic degradation of synthetic dyes. J Environ Chem Eng. 2021;9(4):105776.
[19] Zhang S, Wang Q, Dai F, Gu Y, Qian G, Chen C, et al. Novel $tio_2$ nanoparticles/polysulfone composite hollow microspheres for photocatalytic degradation. Polymers (Basel). 2021;13(3):1–17.
[20] Abdelhameed RM, Shaltout AA, Mahmoud MHH, Emam HE. Efficient elimination of chlorpyrifos via tailored macroporous membrane based on Al-MOF. Sustain Mater Technol. 2021;29:e00326.
[21] Emam HE, El-Shahat M, Abdelhameed RM. Observable removal of pharmaceutical residues by highly porous photoactive cellulose acetate@MIL-MOF film. J Hazard Mater. 2021;414:125509.
[22] Abdelhameed RM, Abdel-Gawad H, Emam HE. Macroporous Cu-MOF@cellulose acetate membrane serviceable in selective removal of dimethoate pesticide from wastewater. J Environ Chem Eng. 2021;9(2):105121.
[23] Abdelhameed RM, El-Shahat M, Emam HE. Employable metal (Ag & Pd)@MIL-125-NH2@cellulose acetate film for visible-light driven photocatalysis for reduction of nitro-aromatics. Carbohydr Polym. 2020;247:116695.
[24] Hayajneh MT, Al-Oqla FM, Al-Shrida MM. Hybrid green organic/inorganic filler polypropylene composites: morphological study and mechanical performance investigations. E-Polymers. 2021;21(1):710–21.
[25] Zare Y, Rhee KY. Analysis of critical interfacial shear strength between polymer matrix and carbon nanotubes and its impact on the tensile strength of nanocomposites. J Mater Res Technol. 2020;9:4123–32.
[26] Hamad QA, Oleiwi JK, Abdulrahman SA. Tensile properties of laminated composite prosthetic socket reinforced by different fibers. Mater Today Proc. 2021. doi: 10.1016/j.matpr.2021.06.348.
[27] Ndukwe CO, Ezurike BO, Okpala PC. Comparative studies of experimental and numerical evaluation of tensile properties of glass fibre reinforced polyester (GFRP) matrix. Heliyon. 2021;7(5):e06887.
[28] Noguchi T, Endo M, Niihara K, Jinnai H, Isogai A. Cellulose nanofiber/elastomer composites with high tensile strength, modulus, toughness, and thermal stability prepared by high-shear kneading. Compos Sci Technol. 2020;188:108005.
[29] Dileep P, Narayanankutty SK. Styrenated phenol modified nanosilica for improved thermo-oxidative and mechanical properties of natural rubber. Polym Test. 2020;82:106302.
[30] Callister WD, Rethwisch DG. Material science and engineering. 9th ed. Hoboken (NJ), USA: John Wiley & Sons; 2014.
[31] Rajeswari A, Christy EJS, Swathi E, Pius A. Fabrication of improved cellulose acetate-based biodegradable films for food packaging applications. Environ Chem Ecotoxicol. 2020;2:107–14.
[32] Vatanpour V, Pasaoglu ME, Barzegar H, Teber OO, Kaya R, Bastug M, et al. Cellulose acetate in fabrication of polymeric membranes: a review. Chemosphere. 2022;295:133914.
[33] Haider AJ, Sultan FI. Structural, morphological and random laser action for dye-Zno nanoparticles in polymer films. Int J Nanoelectron Mater. 2018;11(Special Issue BOND21):97–102.
[34] Ahmed I, Jaber H, Salih S. Electrophoretic deposition used to prepare and analyze the microstructure of chitosan/hydroxyapatite nano-composites. Eng Technol J. 2021;39(11):1693–704.

[35] Jihad MA, Noori FTM, Jabir MS, Albukhaty S, Almalki FA, Alyamani AA. Polyethylene glycol functionalized graphene oxide nanoparticles loaded with nigella sativa extract: A smart antibacterial therapeutic drug delivery system. Molecules. 2021;26:11.
[36] Gao Y, Wang X, Li X, Dai H. Antibacterial composite film based on cellulose acetate/$TiO_2$ nanoparticles. New J Chem. 2020;47:20481–896.
[37] Gonçalves SM, dos Santos DC, Motta JFG, Santos RR, dos, Chávez DWH, Melo NRde. Structure and functional properties of cellulose acetate films incorporated with glycerol. Carbohydr Polym. 2019;209:190–7.
[38] Albukhaty S, Albayati L, Alkaragoly H, Al-Musawi S. Preparation and characterization of titanium dioxide nanoparticles and in vitro investigation of their cytotoxicity and antibacterial activity against Staphylococcus aureus and Escherichia coli. Anim Biotechnol. 2020 Nov;28:1–7. doi: 10.1080/10495398.2020.1842751.
[39] Tang S, Wang Z, Li P, Li W, Li C, Wang Y, et al. Degradable and photocatalytic antibacterial Au-$TiO_2$/sodium alginate nanocomposite films for active food packaging. Nanomaterials. 2018;8:11.
[40] Prakash J, Venkataprasanna KS, Bharath G, Banat F, Niranjan R, Venkatasubbu GD. In-vitro evaluation of electrospun cellulose acetate nanofiber containing Graphene oxide/$TiO_2$/Curcumin for wound healing application. Colloids Surfaces A Physicochem Eng Asp. 2021;627:127166.
[41] Hassan M, Zeid REA, Abou-Elseoud WS, Hassan E, Berglund L, Oksman K. Effect of unbleached rice straw cellulose nanofibers on the properties of polysulfone membranes. Polymers (Basel). 2019 May;11:6.
[42] Mahmoud KH, Elsayed KA, Kayed TS. Optical properties of poly (ethyl methacrylate) – cellulose acetate propionate blend film irradiated with Nd:YAG laser. J Polym Res. 2020;27(4):93.
[43] Sharma A, Mandal T, Goswami S. Fabrication of cellulose acetate nanocomposite films with lignocelluosic nanofiber filler for superior effect on thermal, mechanical and optical properties. Nano-Struct Nano-Obj. 2021;25:100642.
[44] Mansour SA, Farha AH, Kotkata MF. Sol–gel synthesized Co-doped anatase $TiO_2$ nanoparticles: structural, optical, and magnetic characterization. J Inorg Organomet Polym Mater. 2019;29(4):1375–82.
[45] Cruz-González N, Calzadilla O, Roque J, Chalé-Lara F, Olarte JK, Meléndez-Lira M, et al. Study of the effect of $TiO_2$ layer on the adsorption and photocatalytic activity of $TiO_2$-$MoS_2$ heterostructures under visible-infrared light. Int J Photoenergy. 2020;2020:1–9.
[46] Zakir O, Idouhli R, Elyaagoubi M, Khadiri M, Aityoub A, Koumya Y, et al. Fabrication of $TiO_2$ nanotube by electrochemical anodization: toward photocatalytic application. J Nanomater. 2020;2020:1–11.
[47] Kaya M, Khadem S, Cakmak YS, Mujtaba M, Ilk S, Akyuz L, et al. Antioxidative and antimicrobial edible chitosan films blended with stem, leaf and seed extracts of Pistacia terebinthus for active food packaging. RSC Adv. 2018;8(8):3941–50.
[48] Al-Naamani L, Dobretsov S, Dutta J. Chitosan-zinc oxide nanoparticle composite coating for active food packaging applications. Innov Food Sci Emerg Technol. 2016;38:231–7.
[49] Neelapala SD, Nair AK, JagadeeshBabu PE. Synthesis and characterisation of $TiO_2$ nanofibre/cellulose acetate nanocomposite ultrafiltration membrane. J Exp Nanosci. 2017;12(1):152–65.